Carbohydrate Polymers 113 (2014) 615–623

Contents lists available at ScienceDirect

Carbohydrate Polymers

journal homepage: www.elsevier.com/locate/carbpol

Supramolecular transitions in native cellulose-I during progressive oxidation reaction leading to quasi-spherical nanoparticles of 6-carboxycellulose

Priyanka R. Sharma [a], Pattuparambil R. Rajamohanan [b], Anjani J. Varma [a,*]

[a] Polymer Science & Engineering Division, CSIR-National Chemical Laboratory, Pune 411008, India
[b] NMR Resource Center, Organic Chemistry Division, CSIR-National Chemical Laboratory, Pune 411008, India

ARTICLE INFO

Article history:
Received 12 February 2014
Received in revised form 22 July 2014
Accepted 23 July 2014
Available online 1 August 2014

Keywords:
Cellulose
Carboxycellulose
Nanoparticles
WAXRD
NMR

ABSTRACT

Cellulose-I swells considerably in phosphoric acid, and converts to amorphous cellulose via a cellulose-II transition state. Controlled oxidation of cellulose-I to 6-carboxycellulose (6CC) using HNO_3–H_3PO_4–$NaNO_2$ oxidation system led to the selective production of 6CC's of varying carboxyl contents (1.7–22%) as well as various shapes and sizes (macro-sized fibrils of several micron length and/or spherical nanoparticles of 25–35 nm), depending on the reaction conditions. 6CC's having less than 14% carboxyl content were largely in cellulose-II form (WAXRD values in-between cellulose I and cellulose II), whereas at 14–22% the 6CC's were largely amorphous; only trace crystallinity was observed at 19% and 22% carboxyl 6CC. Spherical nanoparticles retained a high degree of crystallinity having cellulose-I structure, whereas the macro-sized fibrils were largely converted to cellulose-II structure. Analysis by WAXRD as well as by CP-MAS ^{13}C NMR studies gave similar conclusions. Reduced molecular weight with progressive oxidation, including presence of oligomers, was also evident from an increase in the reducing-end carbon peak at ~92 ppm. For high oxidation levels (>14%) the NMR 92–96 ppm peaks disappeared on extracting with dilute alkali, due to soluble oligomers being removed.

1. Introduction

Cellulose is the most sustainable and ubiquitous biopolymer molecule available on planet earth. It was the earliest material to be classified as a polymer, nearly 175 years ago. Since then it has engaged generations of chemists, physicists and technologists in unraveling its multi-faceted structural features, conformational analysis, inter-conversion of polymorphs, reactions, and applications. Celluloses obtained from different sources (bacterial, fungal, cotton, hardwood, softwood, agricultural residues, etc.) have greatly different fibril sizes, aspect ratios, molecular weights, and purities, all of which affect their chemical and physical properties (Klemm et al., 2011; Roman & Winter, 2004). In natural form, cellulose occurs as a polymorph known as cellulose-I in which the two cellulose chains are arranged in parallel via hydrogen bonding (Atalla & Vanderhart, 1984; Kroon-Batenburg, Bouma, & Kroon, 1996). Another polymorph, cellulose-II, is generally obtained from cellulose-I by mercerization and regeneration processes (Langan, Nishiyama, & Chanzy, 1999; Langan, Nishiyama, & Chanzy, 2001). In addition to this, several new methods have been developed for converting cellulose-I to cellulose-II. For example, treatment of cellulose I with super critical water, ball milling and dissolution/regeneration from ionic solvents (Sasaki, Adschiri &, Arai, 2003; Zhao et al., 2006; Cheng et al., 2012). Cellulose-II has anti-parallel arrangement of cellulose chains through hydrogen bonding, and cannot revert back to cellulose-I. Strong acids like H_2SO_4, under specific conditions, hydrolyze cellulose in such a way that non-crystalline (amorphous) parts of the semi-crystalline cellulose molecule are removed, and a highly crystalline product, known as microcrystalline cellulose, is produced (Laka, Chernyavskaya, Treimanis, & Faitelson, 2000; Wang & Ding, 2004; Bondenson, Kvien, & Oksman, 2006). Phosphoric acid treatment, on the other hand, leads to swelling of cellulose and dissolution (Percival Zhang, Cui, Lynd, & Kuang, 2006), leading to amorphous cellulose. Swelling and dissolution depends on the concentration of acid, time and temperature (Sharrock, 1988; Wood & Bhat, 1988). One report shows that cellulose swells rapidly in 71–80% phosphoric acid; at 81–85% phosphoric acid concentration dissolution occurs at a temperature of 120 °C. Some studies indicate that the transformation of cellulose-I to amorphous cellulose using phosphoric acid as a solvent occurs via a cellulose-II transition state (Zhang et al., 2009; Percival Zhang et al., 2006). Sulfuric acid

* Corresponding author. Tel.: +91 2025902178; fax: +91 2025902618.
E-mail addresses: aj.varma@ncl.res.in, aj.varma@yahoo.com (A.J. Varma).

http://dx.doi.org/10.1016/j.carbpol.2014.07.056
0144-8617/

treatment of cellulose-I under specific conditions leads to nanofibriller structures with high aspect ratios (Ranby, 1949; Ranby, 1951; Marchessault, Morehead, & Walter, 1959). In another variation, cellulose pretreated with alkali solution followed by squeezing out the alkali and sonicating for 8 h under highly acidic conditions, spherical shaped nanoparticles of cellulose were synthesized (Zhang, Elder, & Ragauskas, 2007). It has been reported that the treatment of microcrystalline cellulose with mixed acid sulfuric acid and hydrochloric acid (3:1) at 68 °C for 10 h produced cellulose nanocrystal as well as spherical cellulose nanoparticles (Wang, Ding, & Cheng, 2007; Wang, Ding, & Cheng, 2008). This appears to be the first instance of the cellulose molecule, a fibrous polymer consisting of bundles of fibrils entwined together, getting converted to a spherical shape. Since then, there have been some more examples of spherical shaped functionalized celluloses, such as aminocelluloses, cellulose acetate and 6-carboxycellulose (Nikolajaski, Wotschadlo, Clement, & Heinze, 2012; Kulterer et al., 2012; Sharma & Varma, 2013; Cheng et al., 2014). Amongst the many derivatives of cellulose which have been investigated, 6-carboxycellulose (6CC) has proved to be of immense interest for its biomedical properties. It was first investigated in 1883, and by the 1940s a variety of preparative methods had been investigated (Witz, 1883; Yackel & Kenyon, 1942; Maurer & Reiff, 1943; Unruh & Kenyon, 1942). The outstanding antimicrobial properties of 6CC were soon utilized in a variety of products like wound gauzes and haemostatic materials (Frantz, Clarke, & Lattes, 1944; Frantz & Lattes, 1945; Martina, Kateřina, Miloslava, Jan, & Ruta, 2009; Lipetskaia & Silver, 2010; Stilwell, Marks, Saferstein, & Wiseman, 1998; Vytrasova et al., 2008; Raymond, 2007; Shani, Shani, Oded, Mruwat, & Shoseyou, 2011, OKCEL1864-034). Due to the industrial importance and commercialization of such products, published literature is replete with patents; consequently there are relatively few papers on these materials (Nooy, Pagliaro, Bekkum, & Besemer, 1997; Nachtkamp et al., 2012; Jewell, Komen, Li, Su, & Weerawarna, 2001; Kenyon & Yackel, 1948).

It should be noted that most studies on oxidation of cellulose are based on oxidation of cellulose-II, due to its higher absorption capacity for physiological fluids, as compared to cellulose-I. However, conversion of native cellulose-I to cellulose-II involves an additional step of treatment with corrosive chemicals (strong aqueous alkali, ionic liquids, cupriethylenediamine hydroxide, formation of cellulose xanthate, etc.). This makes cellulose-II a less environment-friendly material and also adds to the cost. It was our hypothesis that cellulose-I may partially or fully convert to cellulose-II and amorphous cellulose during oxidation using phosphoric acid as a reaction medium, since phosphoric acid is known to swell cellulose (Percival Zhang et al., 2006). This prompted us to explore oxidation of cellulose-I using HNO_3–H_3PO_4–$NaNO_2$ oxidation system and to study the reaction products for their polymorph constitution. During our recently published studies on oxidation of cellulose-I to produce 6-carboxycelluloses, we had succeeded in manipulating the reaction conditions so as to obtain 1.7–22% carboxy content celluloses with controlled shapes and sizes (spherical nanoparticles having particle sizes in the narrow range of 25–35 nm and micron sized fibers) (Sharma & Varma, 2013). These molecules were thoroughly characterized by SEM, TEM, AFM, DLS, TGA, DTG, and solubility studies (Sharma & Varma, 2013; Sharma & Varma, 2014). Now, herein we present our results on WAXRD and solid state CP-MAS ^{13}C NMR of the oxidized reaction products to demonstrate the systematic transformation of cellulose-I to cellulose-II and amorphous cellulose. We also investigated the difference in the crystallinities of nano-6CC and macro-sized 6CC's having the same carboxy contents, produced during the progressive oxidation of cellulose-I in HNO_3–H_3PO_4–$NaNO_2$ system at different temperatures. Many electrical and biochemical properties of polymeric biomolecules are greatly dependent on the morphology of the molecules. For example, enzymatic hydrolysis of cellulose are greatly influenced by its crystallinity (Hall, Bansal, Lee, Realff, & Bommarius, 2010). Adhering of biopolymers like proteins to surfaces is dictated by the surface morphology and surface area; knowledge of these features can aid in designing optimal performances in physiological applications (Kristian, 2006). Crystalline cellulosic surfaces are characterized by strong inter- and intramolecular hydrogen bonding and therefore are more compact and more hydrophobic as compared to amorphous cellulose. Due to the added advantage of surface charges, carboxyl functionalized cellulosic nanoparticles have the potential to be far superior to native un-functionalized cellulose nanoparticles for several applications such as pharmaceutical compositions in cosmetics, drug delivery vehicles, etc. (Wei, Kumar, & Banker, 1996; Bellamy & Holub, 1977; Martina et al., 2009a,b; Zhu, Kumar, & Banker, 2001). Functionalized cellulose in nanoparticle form can extend the utility of 6CC in the fields of nanosensors, biocomposites, optics, electronics, etc. (Klemm, Heublin, Fink, & Bohn, 2005; Klemm et al., 2011). Further, detailed microstructure studies on spherical nanoparticles of carboxyl functionalized cellulosic molecules have never been reported. Our study provides insights into the supra-molecular structural changes occurring during the progress of oxidation of cellulose to produce a series of 6CC's and their nanoparticles. This information will be very useful for developing new or improved biomedical applications of 6CC spherical nanoparticles, since carboxycellulose fibrils have already proven their utility in several biomedical applications.

2. Experimental

2.1. Materials

Cellulose-I was extracted from sugarcane bagasse using our patented process (Varma, 2013). Analytical grade nitric acid (65% conc.), *ortho*-phosphoric acid (85% conc.), sodium nitrite (98.0% purity), and calcium acetate (99.0% purity) were procured from Thomas Baker, Mumbai, India. All these chemicals were used without further purification.

2.2. 6-Carboxycelluloses (6CC) and their spherical nanoparticles

6CC's of varying carboxyl contents were prepared according to a procedure developed by us (Sharma & Varma, 2013). Briefly, the procedure consisted of taking finely powdered cellulose-I and adding an appropriate quantity of acid mixture (2:1 ratio, v/v) of 65% HNO_3 and 85% H_3PO_4 over a period of 5 min. The acid mixture was allowed to get absorbed in the cellulose for 10–15 min at the desired reaction temperature. This was followed by slowly adding powdered $NaNO_2$ (1.4 w/v %). The reaction was performed at four different temperatures: 25 °C, 40 °C, 50 °C and 70 °C. The reaction mixture was quenched by diluting with distilled water (5 times the volume of acid mixture), allowed to settle down for 30 min and then decanting off. The solid part was washed with water and water–methanol mixture (2:1 v/v), then centrifuged at 2000 rpm to remove the solid. The reaction products at 25 °C were obtained as single crops, none of which were nanoparticles. For the reaction at 40 °C (24 h and 48 h), after centrifugation of the liquid–solid mixture at 5000 rpm for 5 min, the solid part was removed (first crop); SEM and TEM analysis showed these to consist of macro-sized fibrils of several microns. The supernatant liquid was removed and centrifuged at 12,000 rpm for 15 min to allow a second crop to separate out; on analysis these were found to be nanoparticles of narrow size distribution (25–35 nm). For the reactions at 50 °C and 70 °C, no solid part remained, and the entire hazy colloidal solution was centrifuged as above to allow the nanoparticles to be collected. In

both these cases the entire product consisted of nanoparticles. The yields of the 6CC products decreased continuously with increase in carboxyl content. Thus for 1.7% carboxyl content, the yield was 84% in a 1 h reaction at 25 °C, decreasing continuously to 45% yield for the 22% carboxyl content 6CC in a 48 h reaction. For the 6CC spherical nanoparticles, the yield was 5% at 40 °C in 24 h reaction, 46% at 50 °C/12 h, and 16% at 70 °C/6 h.

2.2.1. Determination of carboxyl content

The carboxyl content of oxidized cellulose was measured according to the method described by United State Pharmacopoeia (USP) (1995). A 0.5 g of sample was taken and emerged in 50 ml of 2% calcium acetate solution for 30 min. The mixture is then titrated with 0.1 N NaOH (standardized) by using Phenolphthalein as an indicator. The volume of NaOH used was corrected by blank titration. The % carboxyl content in sample was calculated by following formula:

$$\text{Carboxyl content } (\%) = \frac{\text{N} \times V \times MW\,(\text{COOH})}{\text{Wt of sample (mg)}} \times 100$$

where N is the normality of NaOH and V is the volume of NaOH used in titration.

2.3. Reduction of (19.7%) 6CC by $NaBH_4$

Two gram of $NaBH_4$ was dissolved in 10 ml of distilled water in a beaker. 300 mg of 6CC (19.7%) was added slowly to the $NaBH_4$ solution. The reaction was allowed to proceed for 12 h under continuous stirring at room temperature. The sample was completely soluble in $NaBH_4$ solution. The final pH of the reaction mixture was observed to be ~11. The material was dialyzed against distilled water and was freeze dried. This sample was studied by CP-MAS ^{13}C NMR.

2.4. Treatment of 6CC (19.7%) with 0.001N NaOH solution

Ten milliliter of 0.001 N NaOH solution (pH 11) was taken in a beaker and 300 mg of 6CC (19.7%) was slowly added to it. This alkali treatment was carried out for 12 h at room temperature under continuous stirring. The sample was completely soluble in NaOH solution. The product was dialyzed against the distilled water and was freeze dried. This sample was studied by CP-MAS ^{13}C NMR.

It is of interest to point out that isolation of product by centrifugation (see Section 2.2) did not remove the oligomers because our synthesis was in acidic medium, hence the oligomers adhered to the higher molecular weight polymers. However, with alkali treatment, the oligomers solubilized and therefore were removed.

2.5. CP-MAS ^{13}C NMR spectroscopy

Solid state CP-MAS ^{13}C NMR spectra of all samples were obtained at room temperature on a Bruker AV-300 NMR spectrometer operating at a frequency of 75.47 MHz. The instrument was equipped with a 4 mm CP-MAS probe. All spectra were acquired with a spinning speed of 8 KHz using 1 m sec contact time and 5 s relaxation delay. About 1000 transients were collected and processed with a line broadening function of 25 Hz prior to Fourier transformation for sensitivity enhancement. The chemical shifts were referred to the CH_2 carbon of adamantane having a value of 38.48 δ.

2.6. Wide-angle X-ray diffraction (WAXRD)

WAXRD spectra and patterns were collected on a PANalytical X'pert Pro dual goniometer diffractometer. A proportional counter detector was used for low angle experiments. The samples were put on sample holders made of aluminum alloy and flattened with a piece of glass. The Cu Kα radiation was generated at 40 kV and 40 mA (λ = 0.15418 nm) with a Ni filter. The data collection was carried out using a flat holder in Bragg–Brentano geometry (5–60°; 4° min^{-1}). The 2D image was converted into 1D image by the standard software available with the instrument. The crystallinity index (CrI) of the samples was calculated by the following equation 1 (Segal, Creely, Martin, & Conrad, 1959).

$$\text{CrI} = \frac{I_{200} - I_{\text{am}}}{I_{200}} \quad (1)$$

where I_{200} is the intensity of main peak for (2 0 0) lattice diffraction I_{am} is the amorphous region peak intensity evaluated as minimum peak arise between main and secondary peaks of lattice plane (2 0 0) and (1 0 1).

3. Result and discussion

3.1. WAXRD analysis

3.1.1. 6-Carboxycellulose (6CC)

The dried samples of cellulose, 6CC's and 6CC-NP were analyzed by WAXRD and the profiles are shown in Fig. 1. The X-ray diffraction patterns for the various 6CC samples clearly shows that several changes have occurred in their crystallinity and crystallite sizes. For cellulose-I, the intensity of the main crystalline peak for (2 0 0) appears at 2θ = 22.8°, the crystalline (1 0 1) peak appears at 15.8°, and the amorphous region peak appears at 18.7° (Segal et al., 1959; Thygesen, Oddershede, Lilholt, Thomsen, & Stahl, 2005). In the case of cellulose-II the main crystalline peak appears as doublet at 2θ = 21.8° and 20.4° and secondary crystalline peak appears at 12.1°. Similarly, the amorphous peak of cellulose-II is located at 2θ = 16.3° (Park, Baker, Himmel, Parilla, & Johnson, 2010; Kumar, Gupta, Lee & Gupta, 2010). The main peak for (2 0 0) lattice diffraction at 2θ = 22.8° is indicative of the distance between hydrogen-bonded sheets in cellulose-I, while the secondary peaks for (1 0 1) and (1 0 1′) lattice diffraction are related to intermolecular hydrogen bonding. To analyze the effect of acid treatment (H_3PO_4/HNO_3) before adding the main oxidizing agent $NaNO_2$, the WAXRD of that sample was recorded and is referred to as "Control" in Fig. 1 and Table 1. The peak intensity for control at 2θ = 21.8°, 20.4°and 12.3°, was found to be at different positions than the original cellulose (cellulose I). This observed transformation clearly shows the partial conversion of native cellulose-I to cellulose-II prior to oxidation, since the broad peak at 21.8 ends at a point beyond 22.8 (Ago, Endo, & Hirotsu, 2004; Chukwuemeka, Rodriguez, Okhamafe, & Rogers, 2012). The shift of the main peak of cellulose-I from 2θ = 22.8° indicates an expansion of the lattice 2θ = 21.8°; this may be due to the swelling of cellulose fiber, caused by HNO_3/H_3PO_4 treatment. The absence of peak intensity at 2θ = 15.6° (and simultaneous appearance of 12.1° peak) in the control sample corresponding to (1 0 1) plane of cellulose-I indicates the conversion of cellulose-I to cellulose-II. However, the peak intensity corresponding to 2θ = 21.8° and 20.4° are broad as compared to peak intensity corresponding to (2 0 0) lattice plane of cellulose-II, which may be possibly due to partially unchanged lattice plane of cellulose I, or it may be dependent on the particular characteristic of the species of cellulose. Furthermore, there is high probability of preliminary reaction occurring on the surface of cellulose. This is because on treatment with acid (HNO_3/H_3PO_4), cellulose swells to some extent and the swollen part gets transformed to cellulose II polymorph and the un-reacted internal part remains as cellulose I (Sebe, Pichavant, Ibarboure, Chantal Koffi, & Tingaut, 2012; Ranby, 1952). Similarly, the possibility of C6 oxidation on cellulose-II fraction is higher. This was clearly demonstrated by WAXRD studies (and also by ^{13}C CP-MAS NMR analysis; see following section on NMR). Table 1

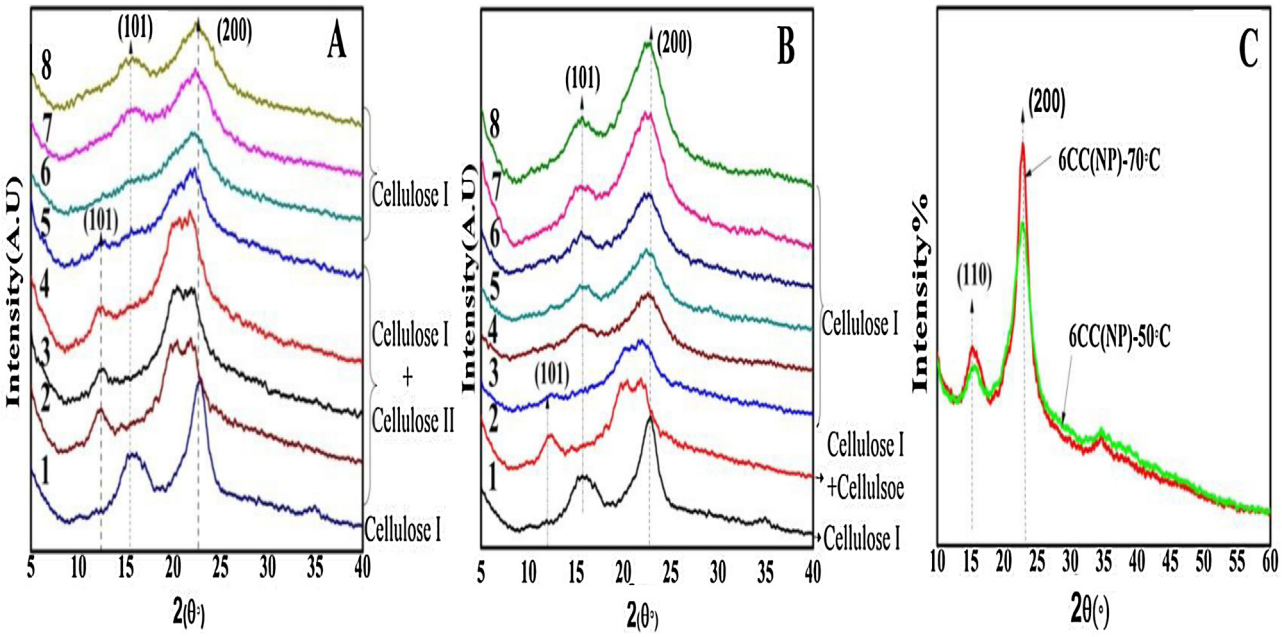

Fig. 1. Overlapping of WAXRD spectra of cellulose and 6CC of various COOH contents (%). (A) Prepared at 25°C: (1) cellulose (2) control (3) 1.7% (4) 3.0% (5) 8.6% (6) 14.1% (7) 19.7% (8) 22.0% carboxyl content. (B) Prepared at 40°C: (1) cellulose (2) controls (3) 6.17% (4) 13.2% (5) 14.3% (6) 14.0% (7) 16.0% (8) 17.0% carboxyl content. (C) 6CC-NP prepared at 50 °C/12 h and 70 °C/8 h.

and Fig. 1 illustrate that the peak intensity related to cellulose-II ($2\theta = 12.2°$) in 6CC of 1%, 3%, 8% carboxyl group content decreases and completely disappears for 6CC of 14% carboxyl content. These results probably indicate that initially on treatment of cellulose with the "solvent system" ($H_3PO_4 + HNO_3$) cellulose-I is partially converted to cellulose-II, which undergoes reactions on the surface; high oxidation levels are achieved on the surface, which get solubilized and are not recovered at the end of the reaction (therefore yields are continuously lower for successive higher degrees of oxidation, up to 14% oxidation) Thereafter, it is noticed that at 14% 6CC and beyond, i.e., for the 19% and 22% 6CC, the peak intensity corresponding to 2θ (200) plane again shifts to $2\theta = \sim 22.3°$ (cellulose I) with a small peak at $2\theta = \sim 15.6°$, which clearly point out the disappearance of cellulose-II polymorph and presence of mostly cellulose-I polymorph. However, the broadening of the peaks from 14% 6CC indicates formation of amorphous cellulose.

3.1.2. Nanoparticles of 6CC

On conversion from macro- to nano-size, cellulose becomes more crystalline due to loss of disordered amorphous region. For 6CC-NP (Fig. 1C), the peak position corresponding to (1 0 1), (1 0 1′) and (2 0 0) lattice plane appeared at 15.4°, 16.5° and 22.9°, respectively, which are similar to the peak position corresponding to the lattice plane of cellulose I (Fig. 1C). This evidence is consistent with the previously reported data that the nano-whiskers of cellulose prepared by sulfuric acid hydrolysis also show greater crystallinity as compared to the starting native cellulose-I (Cheng et al., 2012; Zhang et al., 2009).

3.1.3. Crystallinity index

The crystallinity index (CrI) was calculated by Eq. (1), and the results are shown in Table 2. The CrI calculated for native cellulose-I (extracted from sugarcane bagasse) and 'control' (by treatment of cellulose with $HNO_3 + H_3PO_4$) were 60% and 51%, respectively. The lowest CrI of 34% was obtained for 6CC—48 h/40 °C (Table 1). At 25 °C, there was not much change in the crystallinity up to 6 h reaction time (8.6% —COOH) but sudden drop occurred from reaction times above 12 h. Thus, at 12 h reaction time (14.1% —COOH) a CrI of 39%) and at 48 h reaction time a CrI of 36% was obtained. At the higher reaction temperature of 40 °C, a sudden drop in crystallinity was noticed for 3 h (13.2% —COOH) with CrI of 44%, which decreased steadily to 34% for a reaction time of 48 h (crop I). Interestingly, the 6CC (14–22% —COOH) showed almost similar crystallinity as amorphous cellulose (Ciolacu, Ciolacu, & Popa, 2011). This confirms the formation of amorphous oxidized cellulose 6CC's of high

Table 1
X-ray diffraction patterns and related peak positions corresponding to different lattice plane for cellulose, control*, 6CC's, 6CC-NP and cellulose II.

Planes	2 (θ),0										
	Cellulose I		Control* (H_3PO_4–HNO_3) treated cellulose	6CC 1.7%	6CC 3.0%	6CC 8.6%	6CC 14.1%	6CC 19.7%	6CC 22%	6CC-NP 13.2%	Cellulose II Maize Cob †
	Maize cob†	SBC††									
(1 0 1)	15.0	15.8	12.3	12.3	12.25	12.53 Small	15.6 Very Small	15.6	15.5	15.4	12.5
(1 0 1́)	16.6	16.9	20.4 (Two peaks)	20.4	20.45	20.27	–	–	–	16.5	20.4
(2 0 0)	22.4	22.8	21.8 (Two peaks)	22.0	22.08	22.24	22.13	22.3	22.4	22.9	21.9

† Chukwuemeka et al. (2012).
†† Sugarcane bagasse cellulose prepared by our proprietary method (Varma, 2013).
* Cellulose treated with acid ($HNO_3 + H_3PO_4$ (1:2 ratio) prior to addition of oxidizing agent $NaNO_2$.

Table 2
Degree of crystallinity of cellulose, 6CC's and 6CC-NP of various COOH contents (%).

Reaction time (h)	25 °C	CrI	40 °C	CrI	50 °C (NP)	CrI	70 °C (NP)	CrI
1 h	1.7	55	6.17	55	–	–	–	–
3 h	3.0	52.	13.2	44	–	–	–	–
6 h	8.6	50	14.3	39	–	–	–	–
8 h	–	–	–	–			13.9	63
12 h	14.1	39	14.0	36	13.2	51	–	
24 h								
(I crop)	19.7	38	16.0	35				–
(II crop)			18.0	–				
48 h								
(I crop)	22.0	36	17.0	34	–	–	–	–
(II crop)			21.5	41				

carboxyl content (14–22% COOH). In the same reaction a crop II (40 °C/48 h) was obtained which consisted of nanoparticles of high crystallinity with cellulose-I structure (6CC-NP, 13.2% carboxyl content, Table 2). However, the crystallinity of nanoparticles increased when they were prepared at high temperature. At 50 °C, 6CC-NP (13.2% COOH) showed CrI to 51% and at 70 °C, 6CC-NP (13.9% COOH) showed CrI of 63%, which is higher than the corresponding 6CC non-nanoparticle obtained at 25 °C and 40 °C (Table 2). The increase in crystallinity is further aided by the fact that the amorphous regions of the inner core also hydrolyze away as the reaction proceeds,

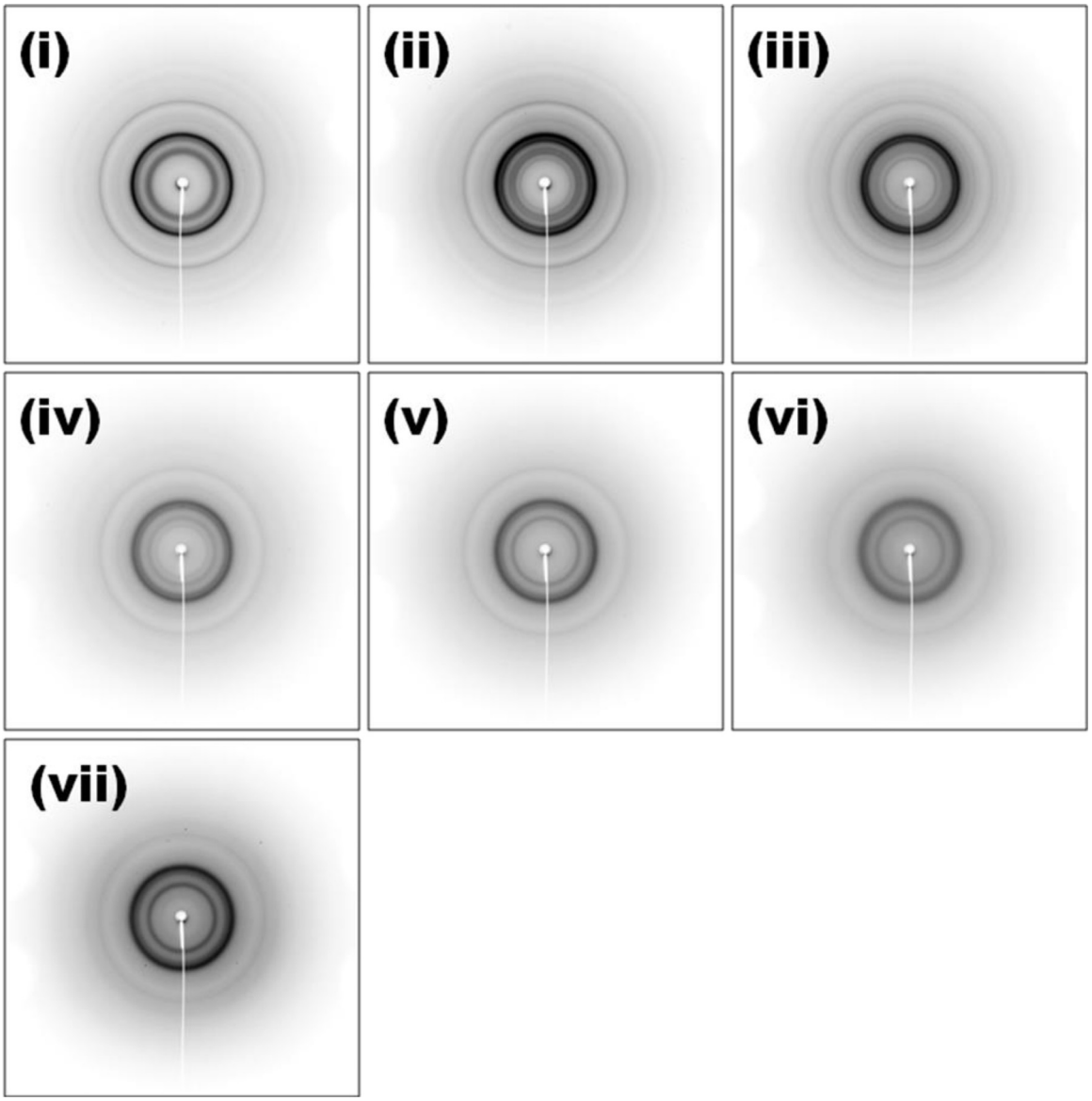

Fig. 2. X-ray diffraction patterns: (i) cellulose (ii) control* (iii) 6CC (3%) (iv) 6CC (8.6%) (v) 6CC (14.1%) (vi) 6CC (19.7%) (vii) 6CC (13.2%)-NP.
* Cellulose treated with HNO_3+H_3PO_4 (1:2) ration prior to addition of oxidizing agent $NaNO_2$.

thereby increasing the crystallinity over the starting cellulose I for the nanoparticles obtained at 70 °C (Fig. 1C).

3.1.4. X-ray diffraction patterns

The interpretation of data from measurements of WAXRD and crystallinity index were confirmed by the pattern of X-ray diffraction in Fig. 2. Interestingly, partial conversion of cellulose-I to cellulose-II is clearly depicted in Fig. 2(i) and (ii). The expansion of lattice plane of cellulose-I is clearly visible in the control sample ($HNO_3 + H_3PO_4$ treated) (Fig. 2(ii). Subsequently, on oxidation almost the same crystallinity is maintained up to 6CC (3%) (Fig. 2(iii) but as the oxidation proceeds the pattern of X-ray diffraction rings became faint (8–14%) (Fig. 2(iv) and (v)) and then completely dull for 6CC (22%) (Fig. 2(vi)). This clearly shows the conversion of most of the cellulose-I to amorphous cellulose. Furthermore, the pattern obtained for 6CC-NP, Fig. 2(vii) showed well defined rings, indicating highly crystalline molecules.

The study conducted provides information on the transformation of cellulose polymorphs during oxidation of native cellulose-I by $HNO_3/H_3PO_4/NaNO_2$. Due to the presence of phosphoric acid as a swelling agent, the progress of the oxidation reaction first led to cellulose-II polymorph until conversion to 6CC with 14% carboxyl, and from 14–22% carboxyl, the cellulose was largely amorphous. Thus, our results support the theory that cellulose-II is the transition state during swelling and dissolution of cellulose-I, finally giving rise to amorphous cellulose. Additionally, the prepared 6CC-NP (~14% carboxyl content) obtained as cellulose-I with crystallinity greater than their macro-sized analogs.

3.2. Solid state NMR studies

The solid state CP-MAS ^{13}C NMR spectra of cellulose and 6CC are presented in Table 3, and Fig. 3. The region between 60 and 70 ppm is assigned to C6 of the primary alcohol group. The next cluster between 70 and 80 ppm is attributed to the C2, C3, and C5 carbons. The region between 80 and 95 ppm is associated with C4 and that between 100 and 110 ppm with the anomeric carbon C1 (Sebe et al., 2012). The signal at ~171 ppm corresponds to the carboxyl group of 6CC. The peak intensity of carboxyl increases simultaneously with increase in carboxyl content, as depicted in Fig. 3.

The peak at about ~92 ppm, assigned to C1 anomeric carbon of reducing end of cellulose, starts increasing from 8% 6CC (peak no. 3 of Fig. 3) and continuously increases with carboxyl content. This indicates lowering of DP with the progress of reaction. To confirm the reason of appearance of peak corresponding to ~94 ppm, the solid state CP-MAS ^{13}C NMR spectra was recorded for the 6CC (19.7%) oxidized sample (Fig. 4A) and compared with 6CC (19.7%) after 0.01 NaOH treatment (Fig. 4B), 6CC (19.7%) after $NaBH_4$ treatment (Fig. 4C) under the same reaction conditions (pH = 10.3 and with continuous stirring for 12 h at room temperature). The absence of ~94 ppm peak in the treated 6CC (19.7%) sample (Fig. 4B and C) clearly shows that the signal is due to oligomeric species. These oligomeric species are most probably soluble in alkali as well as with $NaBH_4$. It is also observed that there is no significant change in the intensity of carboxyl peak ~170 ppm. Only the carboxyl peak at ~172 ppm shifted to higher value ~176 ppm due to the formation of carboxylate anion due to NaOH or $NaBH_4$ treatment. The above experimental data CP-MAS ^{13}C NMR data clearly shows that the peak corresponding to (~92–96 ppm) is due to the presence of oligomers. The solution state CP-MAS ^{13}C NMR study of 6CC (19.7%) and 6CC (22%) in d_6-DMSO at 70 °C clearly shows the absence of peak corresponding to ketonic groups (Fig. S1). The peak at 60 ppm corresponding to C6 decreased significantly for 6CC (22%), perhaps merging with the C2, C3, C5 peaks which get broadened, implying a drastic change in the structure of cellulose (from cellulose-I to amorphous cellulose). We have presented (Table S1 in

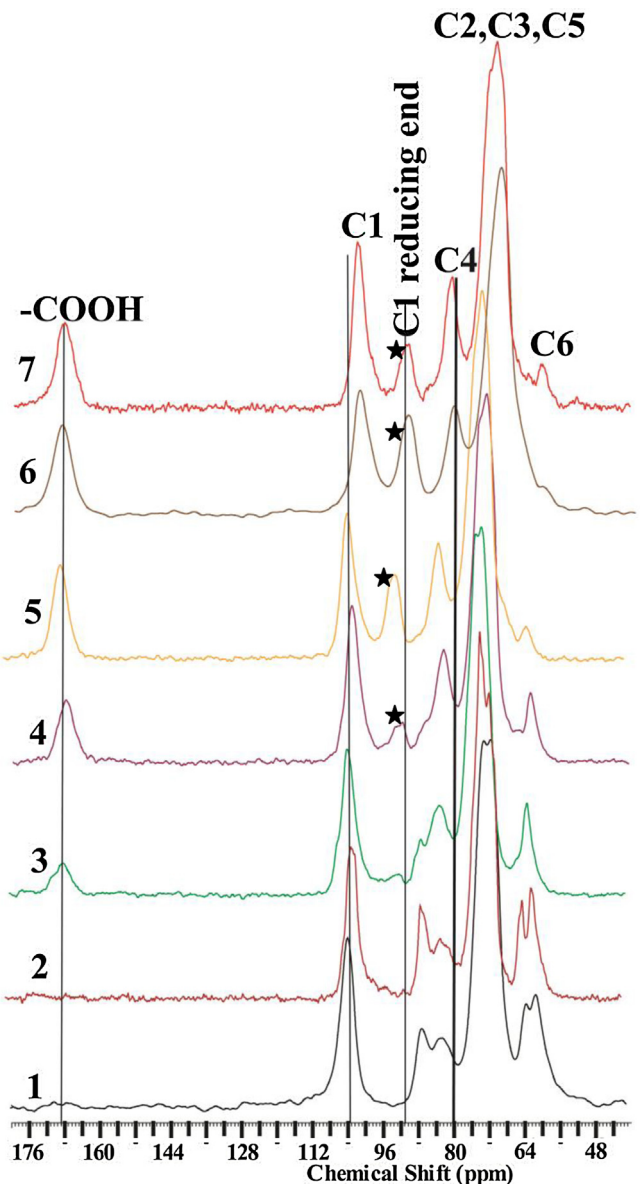

Fig. 3. CP-MAS ^{13}C NMR spectra of (1) cellulose (2) control* (cellulose treated with acid ($HNO_3 + H_3PO_4$ (1:2 ratio) prior to addition of oxidizing agent $NaNO_2$) (3) 6CC (8.6%) (4) 6CC (14.1%) (5) 6CC (19.7%) (6) 6CC (22.0%) (7) 6CC (13.2%)-NP.
♦ The peak disappeared after alkali treatment or NaBH4 reduction reaction.

supplementary data) the integral ratios measured, under identical spectral measurement conditions, CP-MAS ^{13}C NMR for cellulose and oxidized celluloses. It is observed that the integral ratios of peaks at ~105 ppm and ~92 ppm are jointly taken as 1 for the cellulose sample. Similarly, the total integral ratios measured for peaks C2 + C3 + C4 + C6 (90–50) ppm is 4.91 for cellulose. We found that C1: (C2 + C3 + C4 + C5 + C6) ratio varies as the percent oxidation increases in cellulose (The data is shown in Table S1). In case of oxidized celluloses 6CC (8.6%, 14.1% and 19.7%), the total sum of integral area for 105 ppm (original C1 carbon): 92 ppm (C1 reducing end) comes ~1. NMR data was collected under quantitative conditions (Ernst angle of 30° flip angle, 20 s relaxation delay. Maximum T1 observed was 110 s). The CP-MAS spectrum was collected with a contact time of 1 s and relaxation delay of 5 s. Therefore, the calculated NMR integration data clearly shows that the ~92 ppm peak arises due to the C1 reducing end. It is observed that there is not so much change in the integral ratios corresponding to C2 + C3 + C4 + C5 + C6 carbon peaks at (90–50) ppm. The calculated

Table 3
The resonance assignment for the CP-MAS ^{13}C NMR spectra's of cellulose, amorphous cellulose, 6CC's and 6CC-NP of various COOH contents (%).

Carbon atom	Cellulose	Chemical shift (ppm)							
		Control*	6CC (8.6%)	6CC (14.1%)	6CC (19.7%)	6CC (22.0%)	6CC (13.2%)	Cellulose II#	Amorphous cellulose
C1	105.37	103.07 102.21	104.98	104.98	104.98	102.10	102.88	~105	~105
Crystalline C4	89.07	86.79	87.96(s)	87.70(vs)	–	–80.74	–	~86	–
Amorphous C4	84.21	84.09 82.11 80.33	83.51	83.51	83.51	– –	80.87		~83
C2,C3,C5	75.11 72.78	72.85 70.73	75.13 73.83	75.40(m) 73.30	– 73.04(m)	– 70.13	– 72.12 70.55	~75 ~71	75
CrystallineC6	65.38	–	65.45 (s)	65.97(vs)	–	–	–	~61 ppm	–
AmorphousC6	62.84	62.90 60.91	63.09	62.83	63.35(s)	60.85	63.43(s) 60.53		~62
Extra Peaks —COOH Reducing end C1 peak	–	–	171.47 92.94*	169.33 93.20*	172.0 93.98*	169.01 91.09*	169.87 91.45*	~94(C1 reducing end)	

Chukwuemeka et al. (2012).
* Cellulose treated with acid ($HNO_3 + H_3PO_4$ (1:2 ratio) prior to addition of oxidizing agent $NaNO_2$. This peak disappeared on washing in dilute alkaline solution, as was checked in the case of 19.7% 6CC (see Fig. 4).

% oxidation from the solid state CP-MAS ^{13}C NMR analysis shows much higher value as compared to the previous calculated ratio by USP method. The calculated % degradation from these NMR values shows quantitative values of degradation of 6CC's on oxidation to be 15% in 6CC (8.6%), 24% in 6CC (14.1%) and 36% in 6CC (19.7%).

The crystalline peak intensity for C4 carbon atom of cellulose-I appears at ~89 ppm. However, this peak was present in the control sample (Table 3) but gradually decreased for 6CC (8%) and became insignificant for 6CC (14%) and beyond 14%, this peak completely disappeared; now only the peak corresponding to the amorphous region of C4 at ~80–83 ppm was present. Similarly, the crystalline region peak intensity for C6 carbon atom of cellulose I appeared at ~65 ppm. This peak decreased with increase in oxidation and became insignificant for 6CC (14%). For 6CC (>14% carboxyl), only

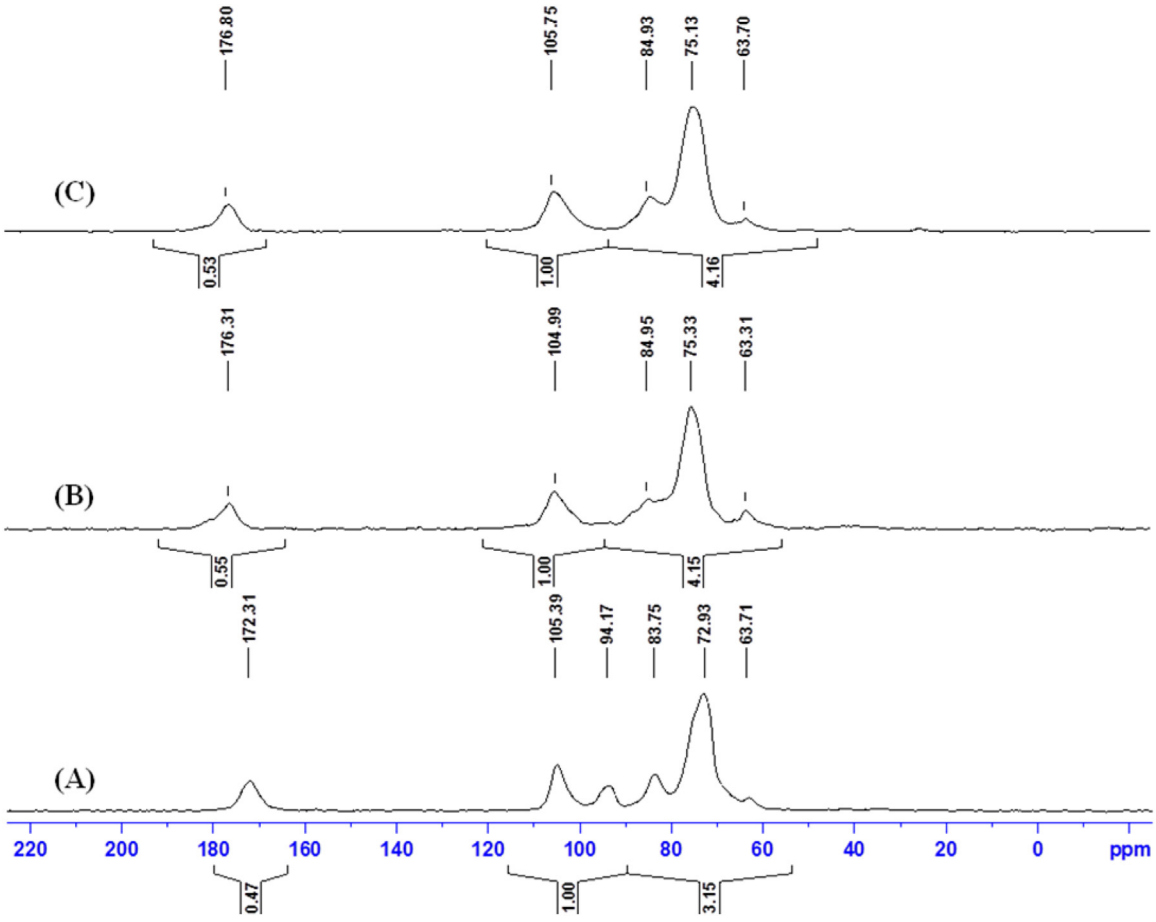

Fig. 4. ^{13}C CP-MAS NMR spectra's of (A) 13 CPMAS of 6CC (19.7%) (B) 13C CPMAS 6CC (19.7%) after 0.01 NaOH treatment (C) ^{13}C CPMAS 6CC (19.7%) after $NaBH_4$ treatment.

the amorphous region of C6 carbon atom was seen, appearing at 63.35 and 60.85 ppm. Thus, solid state CP-MAS ^{13}C NMR analysis shows that for 6CC (>14% carboxyl) mainly the amorphous region of both C4 and C6 carbon exists, with almost no crystalline region. This correlates well with the WAXRD results discussed above. The solid state CP-MAS ^{13}C NMR peaks showed that the 6CC nanoparticles (13.2% carboxyl content) are generally very sharp, and even the carboxyl peak is more enhanced than for 6CC samples having 22% carboxyl groups. This could be due to the rounded shapes and smaller size (25–35 nm) of the molecule in nanoparticle sizes. All other samples of 6CC in Fig. 3 are of macro-sized fibrils.

4. Conclusions

This work has shown that it is possible to use cellulose-I for in-situ preparation of cellulose-II type 6CC materials during the oxidation process using phosphoric acid in the reaction medium. The latter is known to swell cellulose and convert it to amorphous cellulose via cellulose-II transition state. Previously most studies on oxidation of cellulose for biomedical applications are based on oxidation of cellulose-II, due to its higher absorption capacity for physiological fluids. Further, it has been shown that the spherical nanoparticles produced by this synthesis procedure are highly crystalline materials, whereas macro-sized fibrils with the same carboxyl contents have low crystallinities.

Acknowledgement

PRS thanks CSIR, New Delhi, for award of a Senior Research Fellowship leading to a Ph.D. degree.

Appendix A. Supplementary data

Supplementary data associated with this article can be found, in the online version, at http://dx.doi.org/10.1016/j.carbpol.2014.07.056.

References

Ago, M., Endo, T., & Hirotsu, T. (2004). Crystalline transformation of native cellulose from cellulose I to cellulose II polymorph by a ball-milling method with a specific amount of water. *Cellulose*, *11*, 163–167.
Atalla, R. H., & Vanderhart, D. L. (1984). Native cellulose: A composite of two distinct crystalline forms. *Science*, *223*, 283–285.
Bellamy, W. D., & Holub, F. F. (1977). Crystallisation of cellulose (grinding, phosphoric acid). In *US Patent 4,058,411*.
Bondenson, D., Kvien, I., & Oksman, K. (2006). *Strategies for preparation of cellulose whiskers from microcrystalline cellulose as reinforcement in nanocomposites. ACS symposium series* (938) ACS.
Cheng, G., Varanasi, P., Arora, R., Stavila, V., Simmons, B. A., Kent, M. S., & Singh, S. (2012). Impact of ionic liquid pretreatment conditions on cellulose crystalline structure using 1-ethyl-3-methylimidazolium acetate. *Journal of Physical Chemistry B*, *116*, 10049–10054.
Cheng, M., Zongyi, Q., Liu, Y., Yunfeng, Q., Li, T., Chen, L., & Zhu, M. (2014). Efficient extraction of carboxylated spherical cellulose nanocrystals with narrow distribution through hydrolysis of lyocell fibers by using ammonium persulfate as an oxidant. *Journal of Materials Chemistry A*, *2*, 251–258.
Chukwuemeka, P., Rodriguez, A. H., Okhamafe, A. O., & Rogers, R. D. (2012). Physiochemical properties of maize cob cellulose powder reconstituted from ionic liquid solution. *Cellulose*, *19*, 425–433.
Ciolacu, D., Ciolacu, F., & Popa, V. (2011). Amorphous cellulose—Structure and characterization. *Cellulose Chemistry and Technology*, *45*, 13–22.
Frantz, V. K., Clarke, H. T., & Lattes, R. (1944). Experimental studies of alginates as hemostatics. *Annals of Surgery*, *127*(6), 181–198.
Frantz, V. K., & Lattes, R. (1945). Oxidized cellulose—Absorbable gauze. *Journal of the American Medical Association*, *129*(12), 798–801.
Martina, B., Kateřina, K., Miloslava, R., Jan, G., & Ruta, M. (2009). Oxycellulose: Significant characteristics in relation to its pharmaceutical and medical applications. *Advances in Polymer Technology*, *28*(3), 199–208.
Lipetskaia, L., & Silver, D. F. (2010). Laparoscopic use of a hyaluronic acid carboxycellulose membrane slurry in gynecological oncology. *Journal of the Society of Laparoendoscopic Surgeons*, *14*(1), 91–94.
Hall, M., Bansal, P., Lee, J. H., Realff, M. J., & Bommarius, A. S. (2010). Cellulose crystallinity—A key predictor of the enzymatic hydrolysis rate. *FEBS*, *277*, 1571–1582, http://www.okcel.eu/design/okcel/images/Okcel_antimicrobial%20effect.pdf.
Jewell., R. A., Komen, J. L., Li, Y., Su, B., & Weerawarna, S. A. (2001). Method of making carboxylated cellulose fibers and products of the method. In *WO 2001029309 A1*.
Kenyon, W. O., & Yackel, E. C. (1948). Oxidation of cellulose. In *US Patent, 2,448,892*.
Klemm, D., Kramer, F., Moritz, S., Lindstrom, T., Ankerfors, M., Gray, D., & Dorris, A. (2011). Nanocelluloses: A new family of nature-based materials. *Angewandte Chemie International*, *50*, 5438–5466.
Klemm, D., Heublin, B., Fink, H., & Bohn, A. (2005). Cellulose: Fascinating bio[polymer and sustainable raw material. *Angewandte Chemie International*, *44*, 3358–3393.
Kristian, R. (2006). The influence of surface roughness on protein adsorption. In *Ph.D. thesis*. Denmark: Interdisciplinary Nanoscience Center, University of Aarhus.
Kroon-Batenburg, L. M., Bouma, B., & Kroon, J. (1996). Stability of cellulose structures studied by MD simulations. Could mercerized cellulose II be Parallel? *Macromolecules*, *29*, 5695–5699.
Kulterer, M. R., Reichel, V. E., Kargl, R., Kostler, S., Sarbova, V., Heinze, T., Stana-Kleinschek, K., & Ribitsch, V. (2012). Functional polysaccharide composite nanoparticles from cellulose acetate and potential applications. *Advanced Functional Materials*, *22*, 1749–1758.
Kumar, S., Gupta, R., Lee, Y. Y., & Gupta, R. B. (2010). Cellulose pretreatment in subcritical water: Effect of temperature on molecular structure and enzymatic reactivity. *Bioresource Technology*, *101*, 1337–1347.
Laka, M., Chernyavskaya, S., Treimanis, A., & Faitelson, L. (2000). Preparation and properties of microcrystalline cellulose gels. *Cellulose Chemistry and Technology*, *34*, 217–277.
Langan, P., Nishiyama, Y., & Chanzy, H. (2001). X-ray structure of mercerized cellulose II at 1 Å resolution. *Biomacromolecules*, *2*, 410–416.
Langan, P., Nishiyama, Y., & Chanzy, H. (1999). A revised structure and hydrogen-bonding system in cellulose II from a neutron fiber diffraction analysis. *Journal of the American Chemical Society*, *121*, 9940–9946.
Marchessault, R. H., Morehead, F. F., & Walter, N. M. (1959). Liquid crystal systems from fibrillar polysaccharides. *Nature*, *184*, 632–633.
Martina, B., Katerina, K., Miloslava, R., Jan, G., & Ruta, M. (2009). Oxycellulose: Significant characteristics in relation to its pharmaceutical and medical applications. *Advances in Polymer Technology*, *28*, 199–208.
Maurer, V. K., & Reiff, G. (1943). Die oxydation der cellulose init stickstoffdioxyd mitteilung iiber oxydationen mit NO. *Berichte der Deutschen Chemischen Gesellschaft*, *75*(11489), 27–34.
Nachtkamp, K., Kruger, C., Engelhardt, J., Kriegisch, V., Fischer, S., Pinnow, S., & Hettrich, K. (2012). Nanoparticles from slightly oxidized cellulose. In *US Patent 8,338,494*.
Nikolajaski, M., Wotschadlo, J., Clement, J. H., & Heinze, T. (2012). Amino-functionalized cellulose nanoparticles: Preparation, characterization, and interactions with living cells. *Macromolecular Bioscience*, *12*, 920–925.
Nooy, A. E. J., Pagliaro, M., Bekkum, H. V., & Besemer, A. C. (1997). Autocatalytic oxidation of primary hydroxyl functions in glucans with nitrogen oxides. *Carbohydrate Research*, *304*, 117–123.
Park, S., Baker, J. O., Himmel, M. E., Parilla, P. A., & Johnson, D. K. (2010). Cellulose crystallinity index: Measurement techniques and their impact on interpreting cellulose performance. *Biotechnology for Biofuels*, *3*, 1–10.
Percival Zhang, Y. H., Cui, J., Lynd, L. R., & Kuang, L. R. (2006). A transition from cellulose swelling to cellulose dissolution by *o*-phosphoric acid: Evidence from enzymatic hydrolysis and supramolecular structure. *Biomacromolecules*, *7*, 644–648.
Ranby, B. G. (1949). Aqueous colloidal solutions of cellulose micelles. *Acta Chemica Scandinavica*, *3*, 649–650.
Ranby, B. G. (1951). Fibrous macromolecular systems. Cellulose and muscle. The colloidal properties of cellulose micelles. *Discussions of the Faraday Society*, *11*, 158–164.
Ranby, B. G. (1952). The mercerisation of cellulose I. A thermodynamic study. *Acta Chemica Scandinavica*, *6*, 101–105.
Raymond, J. H. (2007). Hemostatic device with oxidized cellulose pad. In *WO143024*.
Roman, M., & Winter, W. T. (2004). Effects of sulfate groups from sulfuric acid hydrolysis on the thermal degradation behavior of bacterial cellulose. *Biomacromolecules*, *5*, 1671–1677.
Sasaki, M., Adschiri, T., & Arai, K. (2003). Production of cellulose II from native cellulose by near- and supercritical water solubilization. *Journal of Agricultural and Food Chemistry*, *51*, 5376–5381.
Sebe, G., Pichavant, F. H., Ibarboure, E., Chantal Koffi, A. L., & Tingaut, P. (2012). Supramolecular structure characterization of cellulose II nanowhiskers produced by acid hydrolysis of cellulose I substrates. *Biomacromolecules*, *13*, 570–578.
Segal, L., Creely, J. J., Martin, A. E. J., & Conrad, C. M. (1959). An empirical method for estimating the degree of crystallinity of native cellulose using the x-ray diffractometer. *Textile Research Journal*, *29*, 786–794.
Shani, N., Shani, Z., Oded, S., Mruwat, R., & Shoseyou, D. (2011). Oxidized cellulose binding to allergens with a carbohydrate-binding module attenuates allergic reactions. *Journal of Immunology*, *186*, 1240–1247.
Sharrock, K. R. (1988). Cellulase assay methods: a review. *Journal of Biochemical and Biophysical Methods*, *17*, 81–105.
Sharma, P. R., & Varma, A. J. (2013). Functional nanoparticles obtained from cellulose: Engineering the shape and size of 6-carboxycellulose. *Chemical Communications*, *49*, 8818–8820.
Sharma, P. R., & Varma, A. J. (2014). Functionalized celluloses and their nanoparticles: morphology, thermal properties, and solubility studies. *Carbohydrate Polymers*, *104*, 135–142.

Stilwell, R. L., Marks, M. G., Saferstein, L., & Wiseman, D. M. (1998). In D. M. Wiseman, D. M. Wiseman, et al. (Eds.), *Handbook of biodegradable polymer*. Amsterdam, B.V.: Overseas Publishers Association.

Thygesen, A., Oddershede, J., Lilholt, H., Thomsen, A. B., & Stahl, K. (2005). On the determination of crystallinity and cellulose content in plant fibres. *Cellulose*, *12*, 563–576.

Unruh, C. C., & Kenyon, W. O. (1942). Investigation of the properties of cellulose oxidized by nitrogen dioxide. *Journal of the American Chemical Society*, *64*, 127–131.

USP (US pharmacopeia 23 National Formulary 18) (1995). Oxidized cellulose.

Varma, A. J. (2013). A process for fractionating sugarcane bagasse into high alpha-cellulose pulp, xylan and lignin. In *China Patent ZL 200880111416*.

Vytrasova, J., Tylsova, A., Brozkove, I., Cervenka, L., Marcela, P., & Havelka, P. (2008). *Antimicrobial effect of oxidized cellulose salts*, *35*, 1247–1252.

Wang, N., & Ding, E. Y. (2004). Thermal behavior of nanocrystalline cellulose treated by acid or alkali. *Acta Polymerica Sinica*, *6*, 925–928.

Wang, N., Ding, E., & Cheng, R. (2007). Thermal degradation behaviours of spherical cellulose nanocrystals with sulfate groups. *Polymer*, *48*, 3486–3493.

Wang, N., Ding, E., & Cheng, R. (2008). Preparation and liquid crystalline properties of spherical cellulose nanocrystals. *Langmuir*, *24*, 5–8.

Wei, S., Kumar, V., & Banker, G. S. (1996). Phosphoric acid mediated depolymerization and decrystallization of cellulose: Preparation of low crystallinity cellulose—A new pharmaceutical excipient. *International Journal of Pharmaceutics*, *142*, 175–18140.

Witz, G. (1883). Oxidation of cellulose. *Bulletin de la Societe industrielle de Mulhouse*, *43*, 334.

Wood, T. M., & Bhat, K. M. (1988). Methods for measuring cellulase activities. *Methods in Enzymology*, *160*, 87–117.

Yackel, E. C., & Kenyon, W. O. (1942). Oxidation of cellulose by nitrogen dioxide. *Journal of the American Chemical Society*, *64*, 121–127.

Zhang, J., Elder, T. J., & Ragauskas, A. J. (2007). Facile synthesis of spherical cellulose nanoparticles. *Carbohydrate Polymers*, *69*, 607–611.

Zhang, J., Zhang, J., Lin, L., Chen, T., Zhang, J., Liu, S., Li, Z., & Ouyang, P. (2009). Dissolution of microcrystalline cellulose in phosphoric acid—Molecular changes and kinetics. *Molecules*, *14*, 5027–5041.

Zhao, H., Kwak, J. H., Wang, Y., Franz, J. A., White, J. M., & Holladay, J. E. (2006). Effects of crystallinity on dilute acid hydrolysis of cellulose by cellulose ball-milling study. *Energy & Fuel*, *20*, 807–811.

Zhu, L., Kumar, V., & Banker, G. S. (2001). Examination of oxidized cellulose as a macromolecular prodrug carrier: Preparation and characterization of an oxidized cellulose–phenylpropanolamine conjugate. *International Journal of Pharmaceutics*, *223*, 35–47.